Two-dimensional pattern analysis and classification using a complex orthogonal estimation algorithm

by

K M Tsang*

and

S A Billings†

*Department of Electrical Engineering
Hong Kong Polytechnic
Hung Hom
Kowloon
Hong Kong

†Department of Automatic Control and Systems Engineering
University of Sheffield
Sheffield S1 3JD
UK

Research Report No 475

Abstract

An orthogonal estimation algorithm is derived for the estimation of parameters associated with the complex autoregressive boundary model of two-dimensional shapes. It is shown that the coefficients of the orthogonal model and the original system parameters are invariant to rotation around the origin, to the choice of starting point in tracing the boundary, and to scale and translation. The error reduction ratios derived from the estimation algorithm can be used to detect which terms should be included in the system model, and classification based on the orthogonal parameters is shown to be less susceptible to incorrect model order specification. Classification based on orthogonal data sets is also derived and it is demonstrated that this approach can avoid some problems associated with classification based on the model parameters alone.

1. Introduction

Closed boundary analysis and shape recognition are basic problems in pattern recognition. Many shape descriptors have been developed (Pavlidis 1980) and Fourier descriptors (Zahn and Roskies 1972), smoothed curvature functions, moments (Dundani et al. 1977), and chord length distributions (You and Jain 1984) are very popular for describing boundaries of different patterns. Recently, Kashyap and Chellappa (1981), Dubois and Glanz (1986) proposed the autoregressive (AR) model approach of analyzing and recognizing two-dimensional shapes which is invariant to rotation, size and translation of the object. In the AR approach, the boundary is approximated by angularly equispaced radius vectors between the boundary and the centroid and an AR model is estimated based on the sequence of radius vectors. Recognition is then performed based on the AR model parameters. However, problems can arise because some boundaries can yield multivalues for some radius vectors (Dubois and Glanz 1986). Furthermore, even though the lengths of the vectors are ordered according to the tracing of the boundary, there is the possibility that different radius shapes give the same ordered lengths (Dubois and Glanz 1986).

To circumvent these problems, Sekita et al. (1992) proposed the complex AR model approach to model the boundary and to recognise the shape based on the complex AR parameters. However the success rate in the recognition of two-dimensional shapes is heavily dependent upon the order of the complex AR model and the number of boundary data points used. Too low or too high a model order might give erroneous results. For example if the number of boundary data points is too large, the estimation algorithm may suffer from numerical problems. However, by adapting the orthogonal estimation algorithm developed by Tsang and Billings (1992) to this problem, the order of the complex AR model can readily be detected using the error reduction ratio. Because of the orthogonality property of the algorithm the fitted orthogonal model parameters will also be invariant to the actual system model order. Hence recognition based on the orthogonal parameters is more robust than with the raw AR model parameters. If the order of the orthogonal parameters is insufficient to capture the characteristics of the boundary data points, more lagged terms can be added to the model with the advantage that the newly introduced parameters will not affect the previously estimated parameters. Hence with the orthogonal parameters and the error reduction ratios, a minimum set of feature vectors can be derived and this will considerably reduce the computational time for the classification of two-dimensional shapes.

The estimation of AR and complex AR models based on the ordinary least squares estimation algorithm can suffer from problems of numerical ill-conditioning if the boundary elements are too close that is if the number of sampled boundary points becomes too large. The

success rate in the recognition of shapes can also start to degrade. Conversely coarse sampling of the boundary data points will lead to a loss of detail in the shapes, there will be large fluctuations in the model parameters and the parameters might be dependent upon the starting point of the boundary tracing. The implementation of the new orthogonal estimation algorithm avoids most of these numerical problems.

To supplement the problem of insufficient characteristics captured by the complex AR parameters, a recognition procedure based on the orthogonal data set is also derived. It is shown that the ratio of the sum of the magnitudes of the orthogonal data vector between the tested and reference patterns provides a useful tool for classifying patterns. Similar shapes give similar magnitude ratios and this ratio test is immune to the sampling interval of the boundary data records as long as the data records capture the essential features of the pattern.

2. Complex autoregressive model representation of boundary

Let $\{\underline{X}(t),\underline{Y}(t)\}$ denote the continuous closed boundary of a two-dimensional shape and let $\{X(k),Y(k),k=0,1,\ldots,N-1\}$ be a sequence of N closed boundary points obtained by sampling $\{\underline{X}(t),\underline{Y}(t)\}$ according to the order of tracing the boundary. For a closed boundary the relationships $X(k)=X(N+k)$ and $Y(k)=Y(N+k)$ hold. The arc length between any two consecutive sampled boundary points is fixed at D and defined as

$$D = \frac{total\ length\ of\ the\ boundary}{N} \tag{1}$$

Hence if the continuous closed boundary is obtained from a frame-grabbler, scanner or computer image, $\{\underline{X}(t),\underline{Y}(t),t=0,1,\ldots,M-1\}$ will denote a sequence of M pixels describing the closed boundary and eqn.(1) can be approximated by

$$d(t) = \sqrt{[\underline{X}(t) - \underline{X}(t-1)]^2 + [\underline{Y}(t) - \underline{Y}(t-1)]^2} \tag{2}$$

$$\underline{X}(-1) = \underline{X}(M-1) \quad , \quad \underline{Y}(-1) = \underline{Y}(M-1)$$

and

$$D = \frac{\sum_{t=0}^{M-1} d(t)}{N} \tag{3}$$

The procedure to sample a sequence of equally spaced boundary points $\{X(k),Y(k),k=0,1,\ldots,N-1\}$ from $\{\underline{X}(t),\underline{Y}(t),t=0,1,\ldots,M-1\}$ can be approximated by the following procedures:-

```
Set     Y(0) = Y(0)
        X(0) = X(0)
        k = 1
        Arc_Length = D
        Distance_Travel = 0
For t = 0 to M - 1
        Distance_Travel = Distance_Travel + d(t)
        If Distance_Travel > Arc_Length
                X(k) = X(t) - [X(t) - X(t-1)]*[Distance_Travel - Arc_Length] / d(t)
                Y(k) = Y(t) - [Y(t) - Y(t-1)]*[Distance_Travel - Arc_Length] / d(t)
                k=k + 1
                Arc_Length = Arc_Length + D
        End
End
```

From the above procedures, a sequence of data records can be collected and an AR model can be fitted to the sampled records $\{X(k), Y(k), k=0,1,\ldots,N-1\}$. The fitted AR models based on the raw data records will be dependent upon transformations of the boundary such as translation, scale, rotation and choice of a starting point in tracing the boundary. To circumvent this, the sampled means are subtracted from the data records to give

$$\begin{aligned} x(k) &= X(k) - \overline{X(k)} \\ y(k) &= Y(k) - \overline{Y(k)} \end{aligned} \tag{4}$$

and a complex variable $z(k)$ is constructed based on $x(k)$ and $y(k)$ such that

$$z(k) = x(k) + jy(k) \tag{5}$$

Hence $z(k)$ will be a sequence of complex numbers that correspond to the boundary points (Fig.1). For the sequence of complex boundary points $z(k)$, a complex AR model of order n is formed by a linear combination of preceding n boundary points as

$$z(k) = \sum_{i=1}^{n} a_i z(k-i) + \epsilon(k) \tag{6}$$

where $\epsilon(k)$ is a complex white noise sequence and $\{a_i, i=1,\ldots,n\}$ are n complex coefficients associated with the lagged boundary points $z(k-i)$. The objective is to identify the unknown coefficients a_i and extract information for pattern analysis.

3. The complex orthogonal estimation algorithm

Sekita et al. (1992) proposed the use of the ordinary least squares estimation algorithm to identify the unknown AR coefficients a_i. However the ordinary least squares estimation

algorithm suffers from numerical instability as the sampled boundary data records get close and the estimated AR coefficients are dependent on the specified model order. The orthogonal least squares estimation algorithm (Korenberg et al. 1988, Billings et al. 1988) has been found to be an effective procedure for identifying unknown linear and nonlinear systems. It is numerically robust and the error reduction ratio test, which is incorporated as part of the algorithm, provides an effective way of identifying the model structure. Tsang and Billings (1992) further extended this algorithm to cover complex number systems.

The complex orthogonal estimation algorithm involves transforming eqn.(6) into an auxiliary equation,

$$z(k) = \sum_{i=1}^{n} g_i w_i(k) + \epsilon(k) \tag{7}$$

where $\{g_i, i=1,\ldots,n\}$ are some constant complex coefficients associated with the orthogonal data set $w_i(k)$ and

$$\overline{w_\kappa^*(k) w_i(k)} = 0 \quad , \quad \kappa \neq i \tag{8}$$

where * denotes complex conjugate and the overbar denotes time averaging. A set of orthogonal data records can be constructed by using the formulae

$$\begin{aligned} w_1(k) &= z(k-1) \\ w_i(k) &= z(k-i) - \sum_{\kappa=1}^{i-1} \alpha_{\kappa i} w_\kappa(k) \quad , \ \kappa < i \\ \alpha_{\kappa i} &= \overline{w_\kappa^*(k) z(k-i)} \ / \ \overline{w_\kappa^*(k) w_\kappa(k)} \quad , \ \kappa = 1,\ldots,i-1 \\ g_i &= \overline{z(k) w_i^*(k)} \ / \ \overline{w_i^*(k) w_i(k)} \quad , \ i = 1,\ldots,n \end{aligned} \tag{9}$$

Notice that the orthogonal coefficients g_i only depend upon the previously fitted orthogonal parameters and will not be affected by the newly included terms. The orthogonal parameters will therefore be invariant to the specified model order. Once g_i have been estimated, the original AR coefficients a_i can be recovered as

$$\begin{aligned} a_n &= g_n \\ a_\kappa &= g_\kappa - \sum_{i=\kappa+1}^{n} \alpha_{\kappa i} a_i \quad , \ \kappa = n-1,\ldots,1 \end{aligned} \tag{10}$$

Equations (9) and (10) define the complex orthogonal least squares estimation algorithm for the analysis of boundary models encoded by complex numbers. The algorithm is remarkably simple and easy to implement and retains all the properties of the original orthogonal least squares algorithm. In fact the transformation of the orthogonal parameters back to the AR

parameters, eqn.(10), may prove to be unnecessary as the characterisation and classification of patterns can be based wholly on the orthogonal parameters. The orthogonal parameters are more robust because they are invariant to the order of the AR model. Hence identification and classification of two-dimensional shapes based on the orthogonal parameters will be investigated. Notice that when the direction (clockwise or counterclockwise) of tracing the boundary data points is different, the complex AR coefficients or the complex orthogonal parameters become complex conjugates of the each other (Sekita et al. 1992).

The error reduction ratio (Tsang and Billings 1992) which is a by-product of the orthogonal least squares estimator, can provide information regarding both the significance of variables in the system model and the adequacy of the fitted model. The percentage reduction in the output variance as a result of including the term $g_i w_i(k)$ into the fitted model can be expressed in terms of the error reduction ratio (Tsang and Billings 1992)

$$\epsilon RR_i = 100 \times g_i g_i^* \overline{w_i^*(k) w_i(k)} \Big/ \overline{z^*(k) z(k)} \tag{11}$$

Hence if the value of the ϵRR_i is large, this would imply that the term $g_i w_i(k)$ is a good candidate to characterise the boundary model and if ϵRR_i is less than a certain threshold, say 0.01, the term can be excluded from the estimation. Also if the sum of the ϵRR_i values for the selected candidate terms is closed to a 100, this would be an indication that the orthogonal model adequately represents the sampled boundary data points.

4. Properties of the complex orthogonal estimation algorithm

Combining the complex orthogonal estimation algorithm with the complex AR model produces some desirable invariant properties. If the boundary is sampled sufficient finely and the boundary is closed, the time averaging values of eqn.(9) will approach the expectation values. Hence α_{ki} and g_i will be invariant to the starting point in tracing the boundary because the sequences are cyclic. If $z(k)$ is represented in polar form $z(k) = r(k)e^{j\theta(k)}$, where $r(k)$ and $\theta(k)$ are the radius and angle vectors respectively, then rotation about the origin by an angle ϕ and scaling by a factor of γ can be expressed as

$$z'(k) = \gamma z(k) e^{j\phi} = \gamma r(k) e^{j(\theta(k)+\phi)} = r'(k) e^{j\theta'(k)} \tag{12}$$

where $z'(k)$ is the new transformed coordinate. Applying the orthogonalisation procedure of eqn.(9) to $z'(k)$ produces

$$
\begin{aligned}
w_1'(k) &= z'(k-1) = \gamma e^{j\phi} z(k-1) \\
w_i'(k) &= z'(k-i) - \sum_{\kappa=1}^{i-1} \alpha_{\kappa i}' w_\kappa'(k) \\
&= \gamma e^{j\phi} \left(z(k-i) - \sum_{\kappa=1}^{i-1} \alpha_{\kappa i}' w_\kappa(k) \right) \qquad , \ \kappa < i \\
\alpha_{\kappa i}' &= \overline{(w_\kappa'(k))^* z'(k-i)} \Big/ \overline{(w_\kappa'(k))^* w_\kappa'(k)} \\
&= \gamma^2 \, \overline{w_\kappa^*(k) z(k-i)} \Big/ \gamma^2 \, \overline{w_\kappa^*(k) w_\kappa(k)} = \alpha_{\kappa i} \ , \ \kappa = 1,\ldots,i-1 \\
g_i' &= \overline{z'(k)(w_i'(k))^*} \Big/ \overline{(w_i'(k))^* w_i'(k)} \\
&= \gamma^2 \, \overline{z(k) w_i^*(k)} \Big/ \gamma^2 \, \overline{w_i^*(k) w_i(k)} = g_i \qquad , \ i = 1,\ldots,n
\end{aligned}
\tag{13}
$$

and hence the parameters $\alpha_{\kappa i}$ and g_i are invariant to scaling and rotation about the origin. From eqn.(13), the scaling factor γ can be recovered from the orthogonal data set as

$$
\gamma = \sum_{k=0}^{N-1} |w_i'(k)| \Big/ \sum_{k=0}^{N-1} |w_i(k)| \tag{14}
$$

Since the starting point of the data sequence is arbitrary and in order to identify the angle of rotation of an object, the alignment of the tested sequence with the reference sequence is required. A cyclic correlation is therefore performed on the radius vector of the tested sequence $r'(k)$ and the reference radius vector $r(k)$ to give

$$
\psi_{r'r}(\tau) = \frac{1}{N} \sum_{k=0}^{N-1} r'(k) r(k+\tau) \quad ; \quad r'(k) = r'(N+k) \ , \ r(k) = r(N+k) \tag{15}
$$

$\psi_{r'r}(\tau)$ will be a maximum if the two sequence are aligned. Once the alignment τ_{max} is found, the angle of rotation can be evaluated as

$$
\theta'(k) - \theta(k+\tau_{max}) = \phi \tag{16}
$$

Hence an estimate of the angle of rotation can be obtained from the orthogonal data records as

$$
\phi = \frac{1}{N} \sum_{k=0}^{N-1} \left(\angle \, w_i'(k) - \angle \, w_i(k+\tau_{max}) \right) \tag{17}
$$

Normally, the angle of rotation is obtained from the first orthogonal data set $w_1(k)$ because higher orthogonal data sets are more susceptible to high frequency variations.

5. Methods of recognising shapes using the complex orthogonal parameters

The concept of "shape" is invariant to any similarly transformation of a pattern. A similarity transformation of a pattern consists of translation, rotation around the centroid and scaling. As mentioned in section 4, the orthogonal parameters are invariant to scale, rotation around the origin and choice of starting point for tracing of the boundary. The orthogonal parameters will be invariant to translation of a boundary if the origin is set at the boundary centroid. To make the orthogonal parameters invariant to the scale of a boundary, the number of boundary points is fixed to a constant N and the boundary points are divided into N segments of equal arc length. It is expected that the orthogonal parameters for the same shape will be identical because they are theoretically invariant to the similarity transformation. Thus shapes could be classified simply by using the Euclidean distance between the tested parameter vector g_i' against the reference vector $\{g_i^c,\ c=1,...,C\}$ such as the feature weighting method or the rotated coordinate system method (Dubois and Glanz 1986) where C is the number of different classes of patterns. The tested boundary points $z'(k)$ are classified as belonging to the class Q if the Euclidean distance between the feature vectors is a minimum

$$\sum_{i=1}^{n} |g_i' - g_i^Q|^2 = \min \left\{ \sum_{i=1}^{n} |g_i' - g_i^c|^2,\ c=1,...,C \right\} \quad \Rightarrow \quad z'(k) \in Q \qquad (18)$$

It has been found that if the sampling interval between the data points is small, most of the minor features can be captured by the sampled data points with the drawback that the variations in the orthogonal or the AR parameters will be insufficient to act as pattern classifiers. For example, the z-transform of the two signals e^{-t} and e^{-2t} are $z/(z-0.999)$ and $z/(z-0.998)$ respectively if the sampling time is 0.001s. There is little difference between the two pulse transfer functions. Hence recognition of two-dimensional shapes based on the system pole locations or the corresponding AR or orthogonal parameters will be difficult if the sampling interval is too small. However, from the magnitude ratio of eqn.(14), the ratio γ is invariant to the sampling interval. In fact smaller sampling intervals will provide better estimates of γ. Hence classification based on the magnitude ratio test is introduced to act as a supplement to feature vector classification.

Define the magnitude ratio for the orthogonal data sets as

$$\gamma_i^c = \sum_{k=0}^{N-1} |w_i'(k)| \Big/ \sum_{k=0}^{N-1} |w_i^c(k)| \quad , \quad i=1,...,n \qquad (19)$$

where $w_i^c(k)$ represents the orthogonal data of the reference data sets. Taking the mean of

the magnitude ratio as a reference, an object is classified as belonging to the class Q if

$$\frac{1}{n}\sum_{i=1}^{n}\left|\frac{\gamma_i^Q - \overline{\gamma^Q}}{\overline{\gamma^Q}}\right| = \min\left\{\frac{1}{n}\sum_{i=1}^{n}\left|\frac{\gamma_i^c - \overline{\gamma^c}}{\overline{\gamma^c}}\right|, c=1,\ldots,C\right\} \Rightarrow z'(k) \in Q \quad (20)$$

where $\overline{\gamma^c}$ is the mean value of γ_i^c.

6. Experiments and results

The effectiveness of the complex orthogonal estimation algorithm for object recognition will be investigated using several examples. The experiments are principally concerned with non-overlapping simply connected planar shapes which are completely known. However, a set of partially occluded shapes are also tested to further illustrate the effectiveness of the new algorithms. The images are binary, and the boundaries are located using a simple boundary following technique (Gonzalez and Wintz 1985). The shapes used to demonstrate classification accuracy are similar to those considered by Dubois and Glanz (1986).

6.1 Data acquisition and description

The shapes used for the experimental portion are illustrated in Figs. 2, 3 and 4. Samples with various sizes, translational and rotational positions were collected. The different sizes were obtained by photocopying and the sizes varied by factors of 0.6, 0.8 and 1.0. The rotation was over the range 0 to 2π rad. Shape set A of Fig. 2 is composed of 9 S's of different sizes and orientations which were used to investigate the effects of the number of sampled data points on the orthogonal parameters and magnitude ratio tests. The error reduction ratio tests as a model order detection tool was also investigated. Shape set B, Fig. 3, is composed of four convex shapes which are relatively similar and serve to test the sensitivity of the shape model to small variations in object shape. Shape set C, Fig. 4, contains eight different objects adopted from industrial shapes. These shapes are relatively complicated, and serve to test the performance of the complex model when used to classify a larger number of classes. The objects were digitised using a HP scanner, different sizes and orientations were obtained by photocopying the images at a scale of 1.0, 0.8 and 0.6. The objects were rotated by arbitrary angles and shifted arbitrarily within the image plane.

6.2 Classification results and discussion

To investigate the effects of the number of sampled points, the starting point of the boundary tracing, translation, size and rotation on the orthogonal parameters and magnitude ratio test, nine pictures obtained from the same pattern with different orientations and sizes were used (Fig. 2). The scaling for pictures (1), (2) and (3) was 1, pictures (4), (5) and (6) were scaled by 0.8 and pictures (7), (8) and (9) by 0.6 respectively. Boundary samples of 20, 50, 100 and 200 points were obtained from the nine pictures and the orthogonal parameter estimation algorithm was applied. Tables 1, 2, 3, and 4 illustrate the first three orthogonal parameters, the corresponding error reduction ratios and the magnitude ratio tests where picture (1) of shape set A was taken as the reference. Table 1 indicates that when the number of data points is small the orthogonal parameters are dependent upon the boundary tracing starting point because the parameters for all nine pictures exhibit large fluctuations especially g_2 and g_3 when N=20. From the error reduction ratio test, the first three orthogonal terms captured around 92 to 95% of the total output information when N=20 indicating around 5 to 8% of the information was not captured by the fitted model. As the number of data records were increased, there was an improvement in the error reduction tests. For N=50, the first three orthogonal parameters captured around 99.7% of the total output indicating that the first three terms were sufficient to describe the pattern as demonstrated by Table 2. As the number was increased to 100 and then 200, the first two orthogonal coefficients were sufficient to capture the characteristics of the pattern because they captured more than 99.97% of the total output. The third orthogonal terms could therefore be excluded from the estimation because these provide a negligible contribution to the total output (Tables 3 and 4). Moreover, as the sampling interval was decreased and the number of sampling boundary points N was increased, the orthogonal parameters were more consistent as illustrated by Tables 2, 3 and 4. The orthogonal coefficients are consistent for large N but they may not discriminate between the patterns because of small differences between different patterns. The parameters will tend to cluster together when the number of data records becomes large. An inspection of the magnitude ratio tests of Tables 1, 2, 3 and 4 however indicates that these are very consistent and are largely invariant to the number of sampled data points. With picture (1) of shape set A taken as reference, the estimated magnitude ratios for all the tested shapes were comparable to the actual values of 1.0, 0.8 and 0.6.

In order to estimate the angle of rotation of an object, picture (9) was selected for the analysis and picture (1) of shape set A Fig. 2 was taken as the reference. The actual scaling of picture (9) compared to picture (1) is 0.6. 200 sampled data points were used for the analysis. From Table 4, picture (9) was found to have a scale of 0.60045 which was the

average magnitude ratios for the first two orthogonal data sets. To evaluate the angle of rotation, a cyclic correlation was performed on the radius vector of pictures (9) and (1) using eqn.(15) and the correlation function is shown in Fig.5. When $\tau = 190$, the correlation function is a maximum and from eqn.(17) the angle of rotation can be evaluated as

$$\phi = \frac{1}{200} \sum_{k=0}^{199} \left(\angle w_1'(k) - \angle w_1(k+190) \right) = -0.3636 \ rad$$

Figure 6 illustrates the transformed sampled boundary data points of picture (9) superimposed on the reference picture (1) after scaling by a factor of 1/0.60045 and a phase correction of -0.3636 radians. A very close match between the two pictures has clearly been obtained and the accuracy of the magnitude ratio tests and the estimated angle of rotation has been demonstrated.

Shape set B of Fig. 3 is composed of four convex shapes which are relatively similar and serve to test the sensitivity of the shape model and magnitude ratio test to small variations in object shapes. 100 boundary data points were collected from each of the shapes shown in Fig. 3 as the reference data. The estimated orthogonal parameters for the four patterns are presented in Table 5. The error reduction ratio tests indicated that a second order model was sufficient to capture the characteristics of the four patterns as sum of the error reduction ratios for all models was over 99.98%. The Euclidean distances between the four orthogonal parameter vectors are shown in Table 6. Clearly, as the sampling interval is reduced the difference in the orthogonal parameters is insufficient to act as a pattern classifier because the difference between the four patterns becomes very small especially between pictures (1) and (4).

Introduction of noise on the collected data may easily corrupt the parameter estimates and result in misclassification. Table 7 shows the result after the magnitude ratio tests were applied to the orthogonal data set where the labelled patterns on each row were taken as the reference. The classification, apart from the test between patterns (2) and (4), based on the magnitude ratio tests is more noticeable in this case because there are large differences in the classification criterion if the object is misplaced. Hence the results obtained by the magnitude ratios tests can supplement the weakness of the orthogonal parameters in pattern classification. Even patterns (2) and (4) which have similar magnitude ratios can be correctly classified if the Euclidean distance of Table 6 is re-applied. Hence coupling the magnitude ratio tests with the orthogonal parameters can form a very powerful pattern classifier.

For the four patterns shown in Fig. 3, 36 patterns of different sizes ranging from 1 to 0.6, rotations and translations were generated and the selection rule of eqn.(20) was coupled with eqn.(15) to perform the pattern classification. All generated patterns were successfully

classified and this clearly demonstrated the effectiveness of the magnitude ratio tests and the orthogonal parameters as pattern classifiers.

Shape set C of Fig. 4 contains eight different objects. These shapes are relatively complicated and serve to test the performance of the orthogonal parameters and the magnitude ratio tests when used to classify a larger number of patterns. 100 boundary points were collected from each pattern shown in Fig. 4 and the first two estimated orthogonal parameters are shown in Table 8. The Euclidean distances between the eight orthogonal parameter vectors are shown in Table 9 and these indicate a similarity between patterns (1) and (3), (1) and (8), (3) and (8), and (6) and (7) because the Euclidean distances between these parameter vectors were small. The magnitude ratio criterion Table 10 indicated that the patterns (1) and (3), (4) and (5), (4) and (8), and (5) and (8) were very similar because the magnitude ratio tests were less than 0.05. A cross reference between the Euclidean distances and the magnitude ratio tests eliminated most of these discrepancies and only patterns (1) and (3) were similar both by the Euclidean distance of the parameter vectors and the magnitude ratio tests. 72 patterns of different sizes, orientations and rotations created from Fig.4 were used to test the classification rule based on the magnitude ratio criterion and the orthogonal parameters. The proposed algorithm correctly classified all the patterns.

The effectiveness of the estimation algorithm in the analysis and classification of partly covered objects was also investigated. Figure 7 shows 32 slightly to moderately covered objects created from the shape set C. 100 boundary data points for each pattern were collected for the analysis. The estimated orthogonal parameters of Table 8 and the magnitude ratio tests of Table 9 for shape set C were taken as reference. Table 11 indicates the Euclidean distances between the 32 estimated parameter vectors and the reference vectors. The minimum Euclidean distance between the tested vector and the reference vectors for each test sample was highlighted by underlining the value and a pattern number with a tagged asterisk indicated that the pattern was incorrectly classified. Table 11 indicates that 8 out of the 32 samples were incorrectly classified and the classification was poor when dealing with patterns (3), (4) and (7). The magnitude ratio test in Table 12 misclassified 12 out of the 32 samples and as above the minimum magnitude criterion for each test sample was underlined. The performance of the magnitude ratio test was particularly poor when dealing with patterns (3), (4) and (8). However taking the magnitude ratio tests as a reference, if the magnitude ratio criterion was higher than 0.1, which is roughly equal to a 10% deviation in the magnitude ratio tests, the test sample should be marked as bad and rejected for further processing. For the remaining test samples, the case which gave the minimum Euclidean distance was therefore considered to be the correct class. This procedure improved the success rate of classification and the misclassified samples were

reduced to 5 as indicated by Table 13. This suggested that the magnitude ratio tests coupled with the orthogonal parameters provide a feasible solution to the classification of slightly covered objects.

7. Conclusions

The complex orthogonal estimation algorithm provides an easy to implement and effective approach for estimating the complex boundary model of two-dimensional shapes. The estimated orthogonal parameters are invariant to model order, size, rotation, translation and starting point in tracing the boundary model. The appropriate model order can also be identified using the error reduction ratio test. The magnitude ratio test derived from the estimation algorithm was shown to overcome some of the weakness associated with just using the orthogonal parameters as pattern classifiers. Coupling the magnitude ratio test with the orthogonal parameters produces a promising way of analysing and classifying two-dimensional non-overlapping and slightly covered objects.

References

BILLINGS, S.A., KORENBERG, M.J., and CHEN, S., 1988, Identification of nonlinear output-affine systems using an orthogonal least squares algorithm, *Int. J. Systems Science*, 19, 1559-1568.

DUBOIS, S.R., and GLANZ, F.H., 1986, An autoregressive model approach to two-dimensional shape classification, *IEEE Trans. Pattern Analysis and Machine Intelligence*, 8, 55-66.

DUNDANI, S.A., BREEDINGS, K.J., and MCGHEE, R.B., 1977, Aircraft identification by moment invariants, *IEEE Trans. Computers*, 26, 39-46.

GONZALEZ, R.C., and WINTZ, P., 1985, *Digital Image Processing*, Englewood Cliffs, NJ: Prentice Hall.

KASYAP, R.L., and CHELLAPPA, R., 1981, Stochastic models for closed boundary analysis: representation and reconstruction, *IEEE Trans. Information Theory*, 27, 627-637.

KORENBERG, M.J., BILLINGS, S.A., and LIU, Y.P., 1988, An orthogonal parameter estimation algorithm for nonlinear stochastic systems, *Int. J. Control*, 48, 193-210.

PAVLIDIS, T., 1980, Algorithm for shape analysis of contours and waveforms, *IEEE Trans. Pattern Analysis and Machine Intelligence*, 2, 301-312.

SEKITA, I., KURITA, T., and OTSU, N., 1992, Complex autoregressive model for shape recognition, *IEEE Trans. Pattern Analysis and Machine Intelligence*, 14, 489-496.

TSANG, K.M., and BILLINGS, S.A., 1992, Orthogonal estimation algorithm for complex number systems, *Int. J. Systems Science*, 23, 1011-1018.

YOU, Z., and JAIN, A.K., 1984, Performance evaluation of shape matching via chord length distribution, *Computer Vision Graphics and Image Processing*, 28, 185-198.

ZAHN, C.T., and ROSKIES, R.Z., 1972, Fourier descriptors for plane closed curves, *IEEE Trans. Computers*, 21, 269-281.

$N=20$	g_1	g_2	g_3	γ_1	γ_2	γ_3	ϵRR_1	$\epsilon RR2$	ϵRR_3	$\Sigma\epsilon RR$
1	.9017+.2226i	-.7087-.0754i	.3977+.3194i	1.0000	1.0000	1.0000	86.2690	6.9750	1.7580	95.0020
2	.8995+.2218i	-.6599-.0563i	.2232+.2228i	0.9995	0.9865	1.0769	85.8350	6.2127	0.7908	92.8385
3	.8980+.2224i	-.6512-.0644i	.2161+.2484i	0.9962	0.9947	1.0891	85.5948	6.1681	0.8929	92.6558
4	.8981+.2221i	-.6605-.0717i	.2405+.2729i	0.7968	0.8041	0.8673	85.5891	6.3620	1.0650	93.0161
5	.8981+.2221i	-.6477-.0617i	.2037+.2379i	0.7965	0.7979	0.8776	85.5976	6.0977	0.8146	92.5099
6	.9018+.2219i	-.7056-.0612i	.3568+.2796i	0.7993	0.7944	0.7995	86.2396	6.9030	1.4094	94.5520
7	.8994+.2218i	-.6760-.0496i	.2706+.2295i	0.5998	0.5917	0.6338	85.8216	6.5139	0.9650	93.3005
8	.8986+.2212i	-.6539-.0513i	.2094+.2219i	0.5995	0.5957	0.6532	85.6398	6.1775	0.7618	92.5791
9	.9011+.2224i	-.7076-.0701i	.3780+.3143i	0.5981	0.6030	0.6066	86.1480	7.0029	1.6552	94.8061

Table 1. Estimated orthogonal parameters, magnitude ratios and error reductio ratios for shape set A, N=20

$N=50$	g_1	g_2	g_3	γ_1	γ_2	γ_3	ϵRR_1	$\epsilon RR2$	ϵRR_3	$\Sigma\epsilon RR$
1	.9830+.0927i	-.9115-.0492i	.5784+.1195i	1.0000	1.0000	1.0000	97.4818	2.0984	0.1465	99.7266
2	.9830+.0927i	-.9104-.0503i	.5987+.1037i	0.9979	1.0003	1.0153	97.4821	2.0933	0.1567	99.7322
3	.9829+.0927i	-.9119-.0507i	.5914+.1201i	0.9963	0.9980	1.0019	97.4739	2.1072	0.1526	99.7336
4	.9829+.0926i	-.9119-.0499i	.5907+.1031i	0.7977	0.8011	0.8095	97.4683	2.1115	0.1511	99.7308
5	.9829+.0926i	-.9108-.0502i	.5946+.1253i	0.7967	0.8003	0.8085	97.4712	2.1043	0.1567	99.7322
6	.9829+.0925i	-.9073-.0475i	.5648+.0936i	0.7979	0.8037	0.8082	97.4561	2.0999	0.1455	99.7016
7	.9828+.0925i	-.9082-.0473i	.5414+.1130i	0.5990	0.6041	0.6059	97.4431	2.1147	0.1353	99.6931
8	.9828+.0925i	-.9075-.0494i	.5526+.1189i	0.5991	0.6043	0.6194	97.4517	2.1051	0.1416	99.6984
9	.9827+.0928i	-.9059-.0495i	.5550+.1134i	0.5975	0.6035	0.6138	97.4410	2.1063	0.1452	99.6925

Table 2. Estimated orthogonal parameters, magnitude ratios and error reductio ratios for shape set A, N=50

$N=100$	g_1	g_2	g_3	γ_1	γ_2	γ_3	ϵRR_1	$\epsilon RR2$	ϵRR_3	$\Sigma\epsilon RR$
1	.9957+.0466i	-.9698-.0237i	.6324-.0424i	1.0000	1.0000	1.0000	99.3559	0.6062	0.0152	99.9773
2	.9957+.0466i	-.9679-.0249i	.5952-.0383i	0.9982	1.0029	1.0556	99.3538	0.6057	0.0144	99.9739
3	.9957+.0466i	-.9686-.0249i	.5929-.0328i	0.9964	0.9994	0.9912	99.3527	0.6077	0.0139	99.9744
4	.9957+.0466i	-.9693-.0244i	.6319-.0501i	0.7977	0.8028	0.8081	99.3508	0.6103	0.0156	99.9767
5	.9957+.0466i	-.9681-.0248i	.5926-.0385i	0.7967	0.8017	0.8170	99.3518	0.6078	0.0142	99.9739
6	.9957+.0466i	-.9674-.0232i	.5795-.0561i	0.7978	0.8035	0.8097	99.3493	0.6093	0.0140	99.9727
7	.9956+.0466i	-.9675-.0238i	.5630-.0236i	0.5989	0.6037	0.6219	99.3464	0.6121	0.0132	99.9717
8	.9956+.0466i	-.9681-.0231i	.6212-.0535i	0.5991	0.6042	0.6362	99.3479	0.6115	0.0158	99.9752
9	.9956+.0467i	-.9670-.0260i	.5685-.0093i	0.5976	0.6035	0.6192	99.3452	0.6127	0.0136	99.9715

Table 3. Estimated orthogonal parameters, magnitude ratios and error reduction ratios for shape set A, N = 100

$N=200$	g_1	g_2	g_3	γ_1	γ_2	γ_3	ϵRR_1	$\epsilon RR2$	ϵRR_3	$\Sigma\epsilon RR$
1	.9989+.0233i	-.9875-.0106i	.4012-.0997i	1.0000	1.0000	1.0000	99.8376	0.1584	0.0007	99.9967
2	.9989+.0233i	-.9866-.0115i	.3874-.0628i	0.9982	1.0028	1.0258	99.8370	0.1587	0.0007	99.9964
3	.9989+.0234i	-.9878-.0113i	.4170-.0742i	0.9965	0.9989	0.9992	99.8370	0.1591	0.0007	99.9968
4	.9989+.0233i	-.9865-.0111i	.3213-.0837i	0.7977	0.8026	0.8679	99.8363	0.1593	0.0005	99.9961
5	.9989+.0233i	-.9877-.0118i	.4429-.0466i	0.7968	0.8012	0.8229	99.8367	0.1593	0.0008	99.9968
6	.9989+.0233i	-.9855-.0105i	.2972-.0467i	0.7977	0.8034	0.8535	99.8358	0.1595	0.0004	99.9957
7	.9989+.0233i	-.9839-.0111i	.1761-.0361i	0.5990	0.6040	0.7437	99.8351	0.1596	0.0002	99.9949
8	.9989+.0233i	-.9844-.0105i	.1943-.0735i	0.5991	0.6043	0.6975	99.8355	0.1594	0.0002	99.9951
9	.9989+.0234i	-.9851-.0118i	.2450-.0589i	0.5975	0.6034	0.6911	99.8348	0.1603	0.0003	99.9954

Table 4. Estimated orthogonal parameters, magnitude ratios and error reductio ratios for shape set A, N=200

pattern	g_1	g_2	ϵRR_1	ϵRR_2	$\Sigma\epsilon RR$
1	.9980+.0598i	-.9656-.0155i	99.9526	0.0442	99.9968
2	.9978+.0564i	-.9486+.0116i	99.8801	0.1079	99.9880
3	.9980+.0627i	-.7117+.0767i	99.9968	0.0016	99.9984
4	.9977+.0595i	-.9760-.0147i	99.8895	0.1053	99.9948

Table 5. Estimated orthogonal parameters and error reductio ratios for shape set B, N=100

pattern	1	2	3	4
1	0.0000	0.0010	0.0730	0.0001
2	0.0010	0.0000	0.0604	0.0015
3	0.0730	0.0604	0.0000	0.0782
4	0.0001	0.0015	0.0782	0.0000

Table 6. Euclidean distances between different pictures of shape set B, N=100

pattern	1		2		3		4	
1	1.0000	0.0000	1.1022	0.2235	1.0996	0.6168	1.1935	0.1918
	1.0000		1.7368		0.2606		1.7599	
2	0.9073	0.2235	1.0000	0.0000	0.9977	0.7386	1.0828	0.0332
	0.5758		1.0000		0.1500		1.0133	
3	0.9094	0.6168	1.0023	0.7386	1.0000	0.0000	1.0854	0.7231
	3.8375		6.6650		1.0000		6.7538	
4	0.8379	0.1918	0.9235	0.0332	0.9214	0.7231	1.0000	0.0000
	0.5682		0.9869		0.1481		1.0000	

γ_1	$\frac{1}{2}\sum_{i=1}^{2}\left\lvert\frac{\gamma_i-\bar{\gamma}}{\bar{\gamma}}\right\rvert$
γ_2	

Table 7. Magnitude ratios for shape set B, N=100

pattern	g_1	g_2
1	0.9952+0.0531i	-.9120+0.0289i
2	0.9879+0.0605i	-.7542-0.0490i
3	0.9950+0.0522i	-.9235+0.0070i
4	0.9969+0.0460i	-.8823+0.0076i
5	0.9973+0.0474i	-.9866-0.0229i
6	0.9967+0.0630i	-.8268+0.0561i
7	0.9976+0.0608i	-.8229+0.0680i
8	0.9973+0.0395i	-.9269+0.0050i

Table 8. Estimated orthogonal parameters for shape set C, N = 100

pattern	1	2	3	4	5	6	7	8
1	0.0000	0.0311	0.0006	0.0014	0.0083	0.0081	0.0095	0.0010
2	0.0311	0.0000	0.0319	0.0199	0.0550	0.0164	0.0185	0.0333
3	0.0006	0.0319	0.0000	0.0017	0.0049	0.0119	0.0139	0.0002
4	0.0014	0.0199	0.0017	0.0000	0.0118	0.0057	0.0074	0.0020
5	0.0083	0.0550	0.0049	0.0118	0.0000	0.0320	0.0352	0.0044
6	0.0081	0.0164	0.0119	0.0057	0.0320	0.0000	0.0002	0.0132
7	0.0095	0.0185	0.0139	0.0074	0.0352	0.0002	0.0000	0.0152
8	0.0010	0.0333	0.0002	0.0020	0.0044	0.0132	0.0152	0.0000

Table 9. Euclidean distances between the orthogonal parameters for shape set C, N = 100

pattern	1	2	3	4	5	6	7	8
1	0.0000	0.2862	0.0285	0.1131	0.1786	0.3399	0.4870	0.1175
2	0.2862	0.0000	0.2598	0.3867	0.4422	0.5705	0.6786	0.3906
3	0.0285	0.2598	0.0000	0.1411	0.2061	0.3648	0.5085	0.1455
4	0.1131	0.3867	0.1411	0.0000	0.0669	0.2358	0.3957	0.0045
5	0.1786	0.4422	0.2061	0.0669	0.0000	0.1716	0.3378	0.0624
6	0.3399	0.5705	0.3648	0.2358	0.1716	0.0000	0.1764	0.2316
7	0.4870	0.6786	0.5085	0.3957	0.3378	0.1764	0.0000	0.3919
8	0.1175	0.3906	0.1455	0.0045	0.0624	0.2316	0.39919	0.0000

Table 10. Magnitude ratio criterion for shape set C, N = 100

pattern	1	2	3	4	5	6	7	8
1.1	0.00015	0.03000	0.00130	0.00140	0.01060	0.00640	0.00750	0.00180
1.2	0.00004	0.03160	0.00036	0.00140	0.00730	0.00900	0.01060	0.00065
1.3	0.00030	0.03580	0.00035	0.00240	0.00570	0.01150	0.01310	0.00046
1.4	0.00007	0.03000	0.00110	0.00130	0.00980	0.00680	0.00810	0.00150
2.1	0.03350	0.00012	0.03480	0.02200	0.05940	0.01690	0.01880	0.03620
2.2	0.02320	0.00006	0.02410	0.01370	0.04530	0.01140	0.01340	0.02530
2.3	0.03090	0.00045	0.03270	0.02000	0.05790	0.01380	0.01540	0.03420
2.4	0.01620	0.00270	0.01620	0.00840	0.03320	0.00980	0.01210	0.01710
3.1*	0.00002	0.03140	0.00079	0.00150	0.00870	0.00790	0.00920	0.00110
3.2	0.00075	0.03450	0.00016	0.00260	0.00450	0.01270	0.01480	0.00056
3.3	0.00110	0.03410	0.00009	0.00240	0.00370	0.0140	0.01620	0.00014
3.4*	0.00009	0.03200	0.00032	0.00150	0.00700	0.00950	0.01110	0.00050
4.1	0.00089	0.02340	0.00240	0.00068	0.01400	0.00380	0.00490	0.00290
4.2	0.00083	0.02440	0.00068	0.00031	0.00840	0.00830	0.01010	0.00077
4.3*	0.00096	0.02660	0.00030	0.00081	0.00650	0.01030	0.01240	0.00041
4.4*	0.00058	0.02720	0.00024	0.00072	0.00680	0.00950	0.01150	0.00038
5.1	0.00530	0.05030	0.00280	0.00870	0.00037	0.02610	0.02890	0.00250
5.2	0.00510	0.04880	0.00260	0.00820	0.00041	0.02550	0.02830	0.00220
5.3	0.00800	0.05290	0.00460	0.01100	0.00004	0.03110	0.03440	0.00400
5.4	0.00440	0.05070	0.00250	0.00830	0.00083	0.02440	0.02700	0.00230
6.1	0.00740	0.01570	0.01090	0.00500	0.03040	0.00003	0.00033	0.01220
6.2*	0.00220	0.01910	0.00390	0.00110	0.01750	0.00220	0.00330	0.00480
6.3	0.00650	0.01380	0.00930	0.00360	0.02770	0.00035	0.00098	0.01050
6.4	0.00680	0.01430	0.00980	0.00410	0.02860	0.00022	0.00075	0.01100
7.1*	0.00016	0.02730	0.00095	0.00086	0.01000	0.00640	0.00780	0.00150
7.2*	0.00480	0.01930	0.00790	0.00350	0.02520	0.00046	0.00085	0.00900
7.3	0.01230	0.01910	0.01730	0.00990	0.04050	0.00062	0.00018	0.01870
7.4	0.01060	0.02700	0.01600	0.01020	0.03760	0.00150	0.00082	0.01730
8.1	0.00260	0.0400	0.00091	0.00450	0.00190	0.01890	0.02130	0.00052
8.2	0.00130	0.03970	0.00047	0.00370	0.00320	0.01560	0.01760	0.00034
8.3	0.00250	0.03920	0.00084	0.00420	0.00220	0.01830	0.02070	0.00043
8.4*	0.00056	0.03810	0.00072	0.00290	0.00580	0.01220	0.01370	0.00062

Table 11. Euclidean distances between the tested orthogonal parameter vectors of shape set D and reference parameter vectors for shape set C, N = 100
(* - incorrectly classified sample)

pattern	1	2	3	4	5	6	7	8
1.1	0.0168	0.3016	0.0453	0.0964	0.1623	0.3249	0.4741	0.1009
1.2	0.0100	0.2770	0.0185	0.1229	0.1883	0.3486	0.4946	0.1273
1.3	0.0024	0.2839	0.0261	0.1155	0.1810	0.3420	0.4889	0.1199
1.4*	0.0630	0.3429	0.0913	0.0505	0.1170	0.2830	0.4375	0.0550
2.1	0.2570	0.0315	0.2302	0.3596	0.4165	0.5489	0.6612	0.3635
2.2	0.2558	0.0327	0.2290	0.3585	0.4155	0.5480	0.6605	0.3624
2.3	0.2424	0.0470	0.2154	0.3460	0.4036	0.5380	0.6524	0.3500
2.4	0.2340	0.0559	0.2069	0.3381	0.3961	0.5316	0.6472	0.3421
3.1*	0.0041	0.2824	0.0244	0.1171	0.1826	0.3435	0.4901	0.1216
3.2*	0.0740	0.3527	0.1022	0.0394	0.1061	0.2727	0.4285	0.0439
3.3*	0.0095	0.2774	0.0190	0.1224	0.1878	0.3482	0.4942	0.1269
3.4	0.0621	0.2281	0.0337	0.1740	0.2381	0.3936	0.5330	0.1783
4.1*	0.1618	0.4281	0.1894	0.0496	0.0174	0.1884	0.3531	0.0451
4.2*	0.1341	0.4047	0.1620	0.0213	0.0456	0.2156	0.3776	0.0169
4.3*	0.1234	0.3956	0.1513	0.0104	0.0565	0.2259	0.3869	0.0059
4.4*	0.1170	0.3901	0.1450	0.0040	0.0629	0.2320	0.3923	0.0005
5.1	0.1961	0.4566	0.2233	0.0849	0.0181	0.1540	0.3217	0.0804
5.2	0.1648	0.4307	0.1924	0.0527	0.0142	0.1854	0.3503	0.0482
5.3*	0.1398	0.4095	0.1676	0.0271	0.0399	0.2101	0.3726	0.0226
5.4	0.2399	0.4922	0.2665	0.1303	0.0640	0.1089	0.2799	0.1259
6.1	0.3544	0.5816	0.3790	0.2513	0.1876	0.0165	0.1603	0.2471
6.2	0.4063	0.6203	0.4298	0.3073	0.2454	0.0771	0.1007	0.3032
6.3	0.2707	0.5168	0.2969	0.1626	0.0967	0.0762	0.2492	0.1582
6.4	0.4001	0.6158	0.4237	0.3006	0.2385	0.0697	0.1080	0.2965
7.1	0.4178	0.6288	0.4411	0.3198	0.2585	0.0909	0.0869	0.3158
7.2	0.5284	0.7076	0.5487	0.4417	0.3863	0.2299	0.0558	0.4381
7.3	0.4931	0.6829	0.5144	0.4025	0.3448	0.1841	0.0080	0.3987
7.4	0.4253	0.6342	0.4483	0.3279	0.2669	0.0998	0.0779	0.3239
8.1*	0.1536	0.4212	0.1812	0.0412	0.0258	0.1966	0.3604	0.0367
8.2*	0.1589	0.4257	0.1866	0.0467	0.0203	0.1913	0.3556	0.0422
8.3*	0.0926	0.3690	0.1207	0.0207	0.0875	0.2553	0.4131	0.0252
8.4	0.1235	0.3956	0.1514	0.0105	0.0564	0.2259	0.3868	0.0060

Table 12. Magnitude ratio criterion for shape set D, N = 100
(* - incorrectly classified sample)

pattern	1	2	3	4	5	6	7	8
1.1	0.00015		0.00130	0.00140				0.00180
1.2	0.00004		0.00036					
1.3	0.00030		0.00035					
1.4	0.00007		0.00110	0.00130				0.00150
2.1		0.00012						
2.2		0.00006						
2.3		0.00045						
2.4		0.00270						
3.1*	0.00002		0.00079					
3.2	0.00075		0.00016	0.00260	0.00450			0.00056
3.3	0.00110		0.00009					
3.4*	0.00009		0.00032					
4.1				0.00068	0.01400			0.00290
4.2				0.00031	0.00840			0.00077
4.3*				0.00081	0.00650			0.00041
4.4*				0.00072	0.00680			0.00038
5.1				0.00870	0.00037			0.00250
5.2				0.00820	0.00041			0.00220
5.3				0.01100	0.00004			0.00400
5.4					0.00083	0.02440		
6.1						0.00003		
6.2						0.00220	0.00330	
6.3					0.02770	0.00035		
6.4						0.00022	0.00075	
7.1*						0.00640	0.00780	
7.2							0.00085	
7.3							0.00018	
7.4						0.00150	0.00082	
8.1				0.00450	0.00190			0.00052
8.2				0.00370	0.00320			0.00034
8.3	0.00250			0.00420	0.00220			0.00043
8.4				0.00290	0.00580			0.00062

Table 13. Cross reference test for shape set D
(* - incorrectly classified sample)

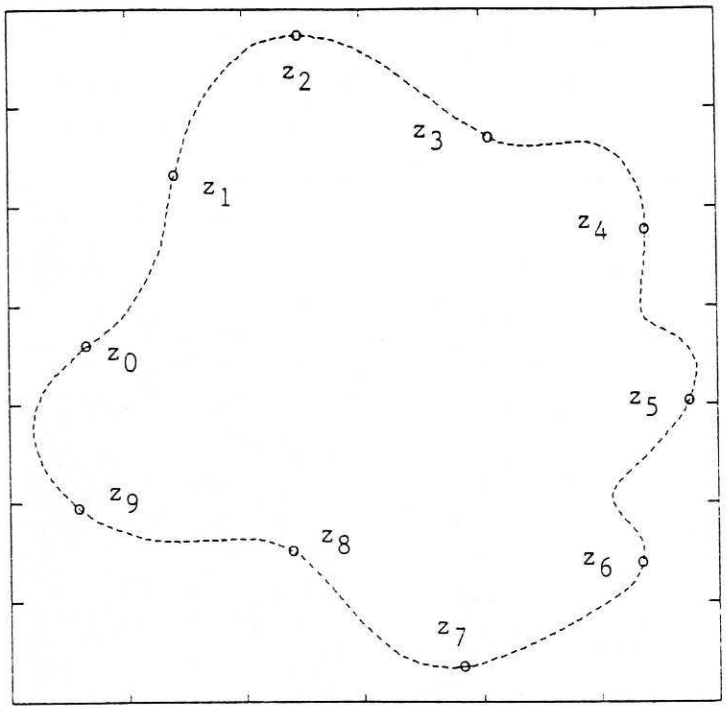

$$z_i = x_i + jy_i$$

Figure 1. Complex boundary coordinates

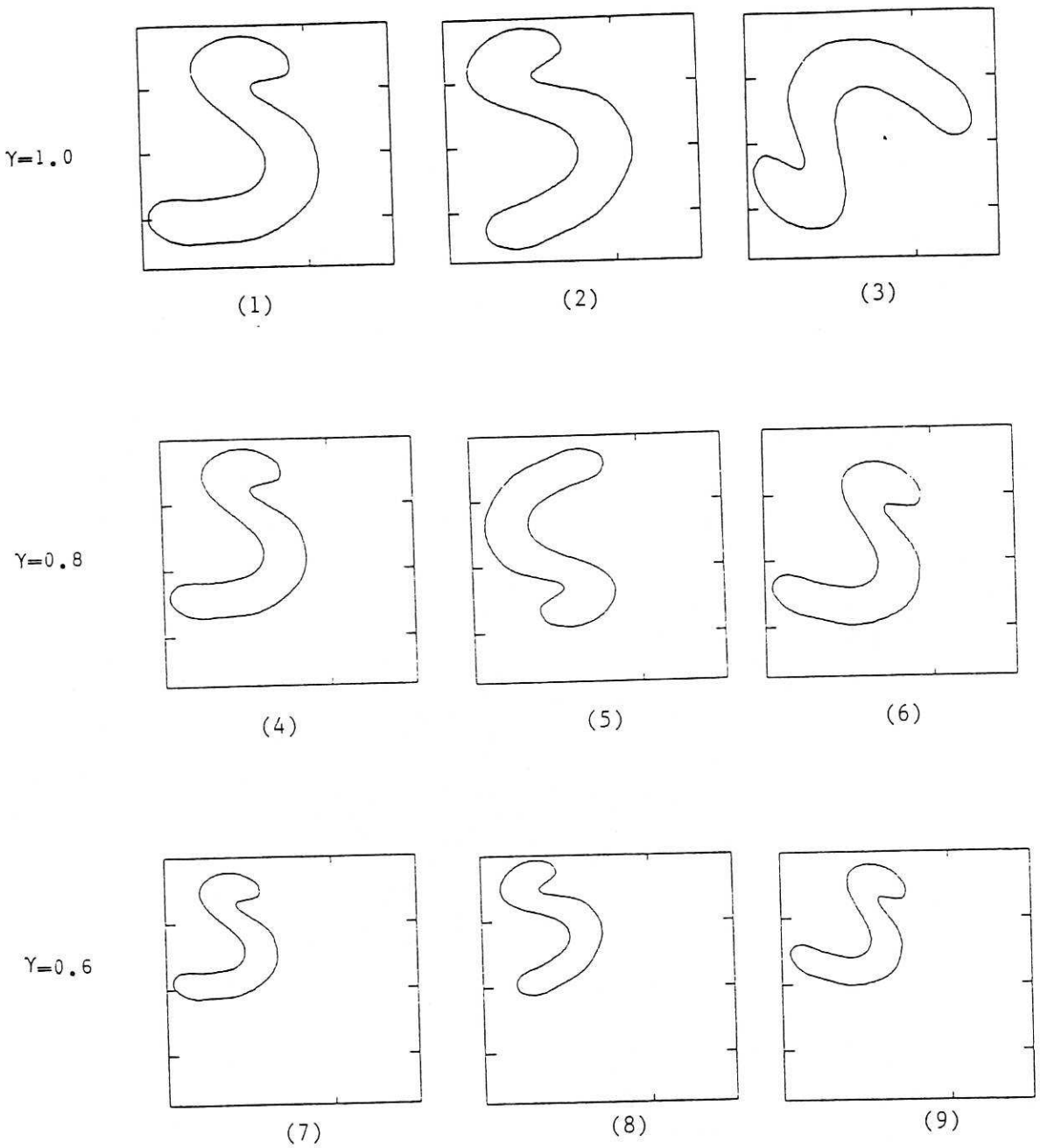

Figure 2. Shape set A

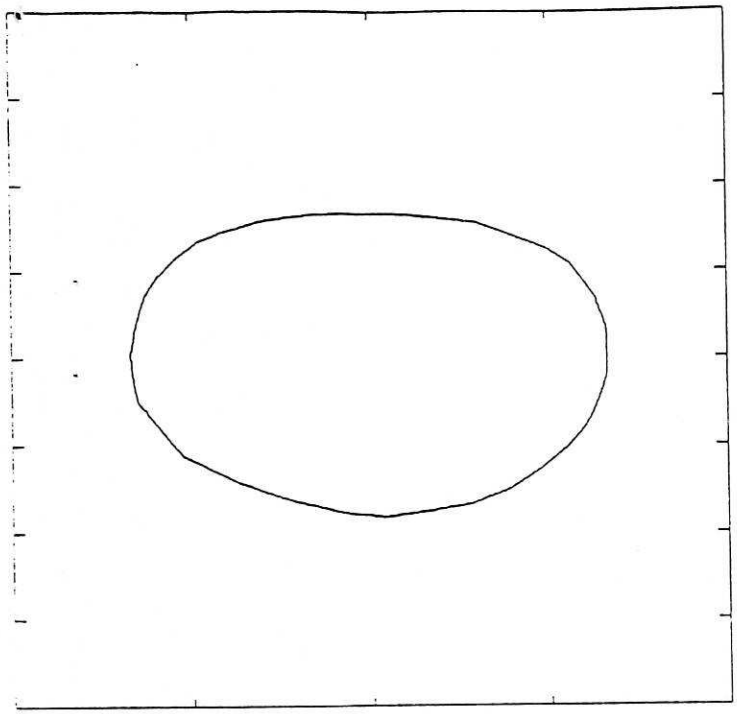

(1)

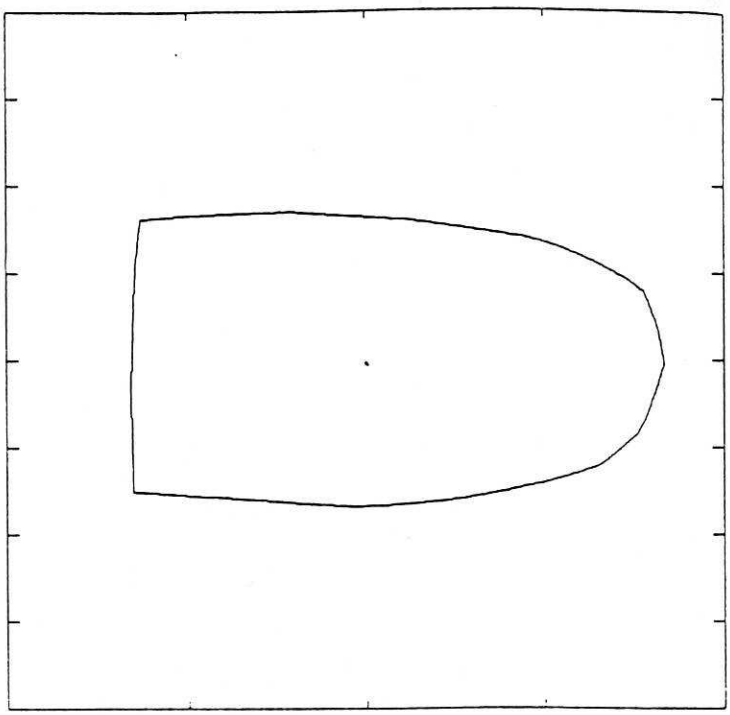

(2)

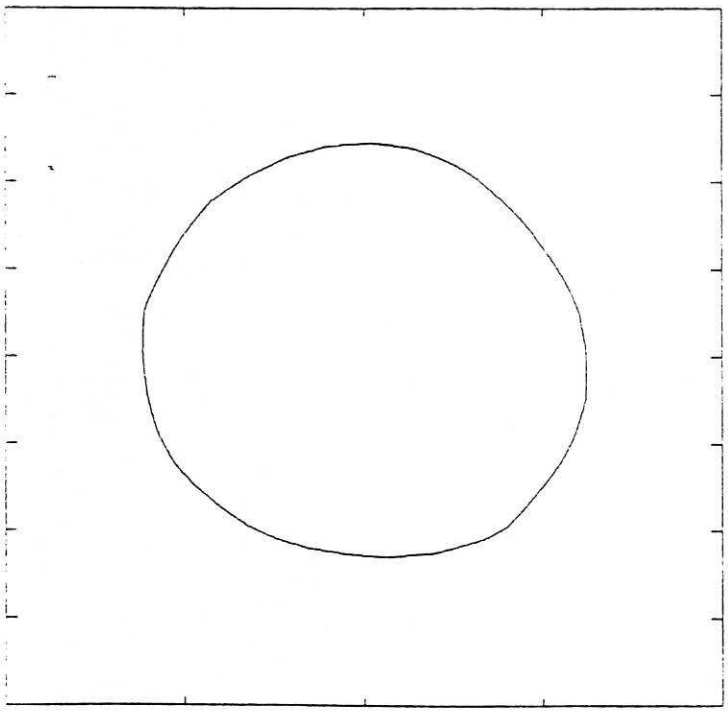

(3)

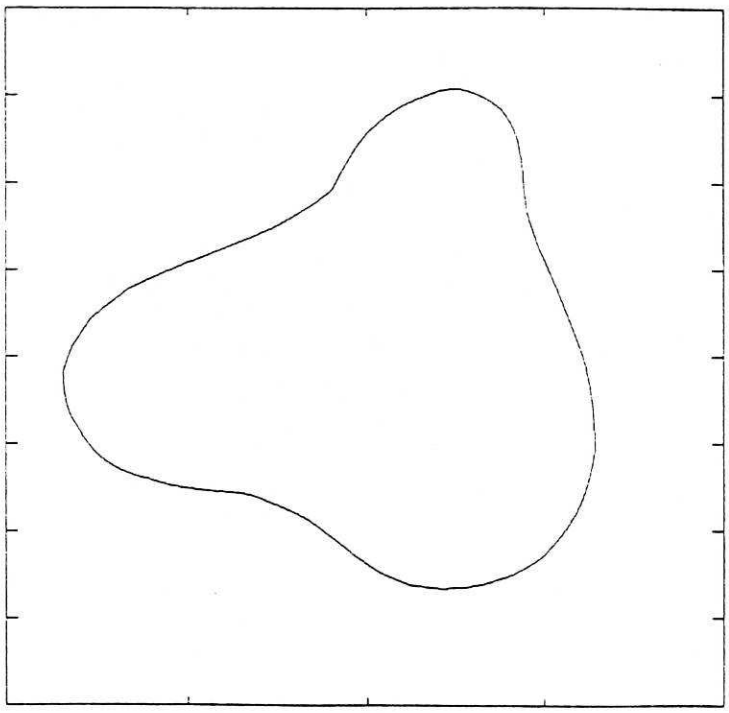

(4)

Figure 3. Shape set B

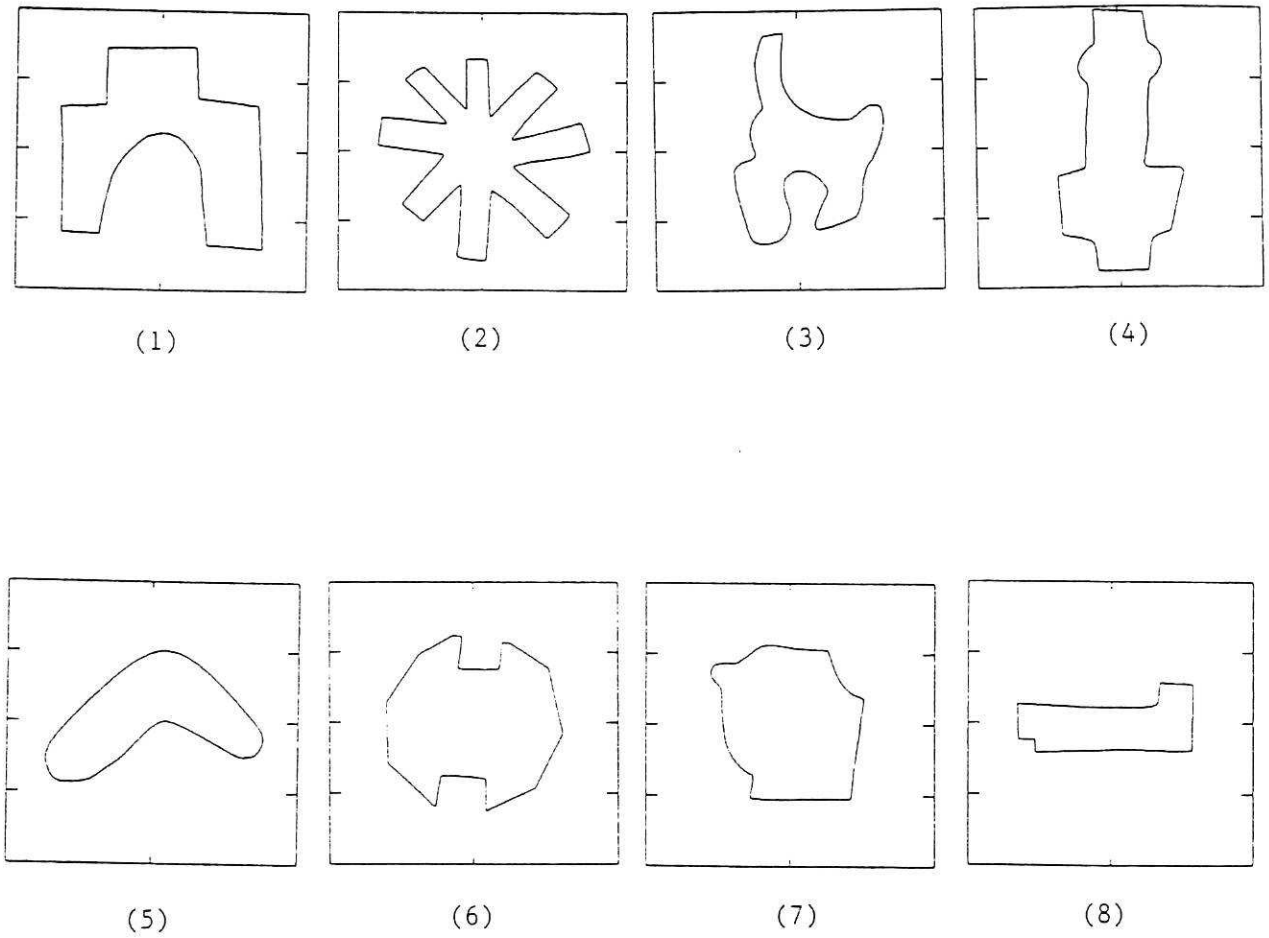

Figure 4. Shape set C

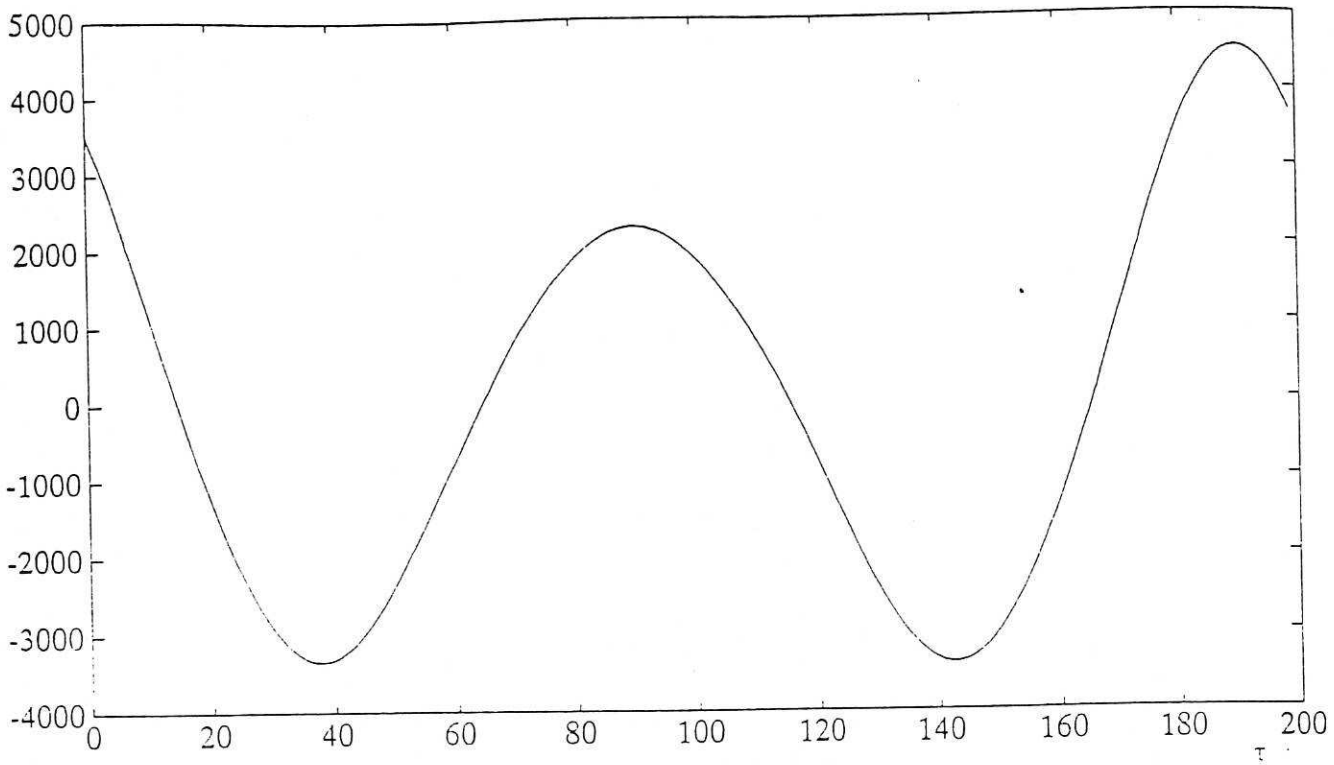

Figure 5. Cross-correlation function plot

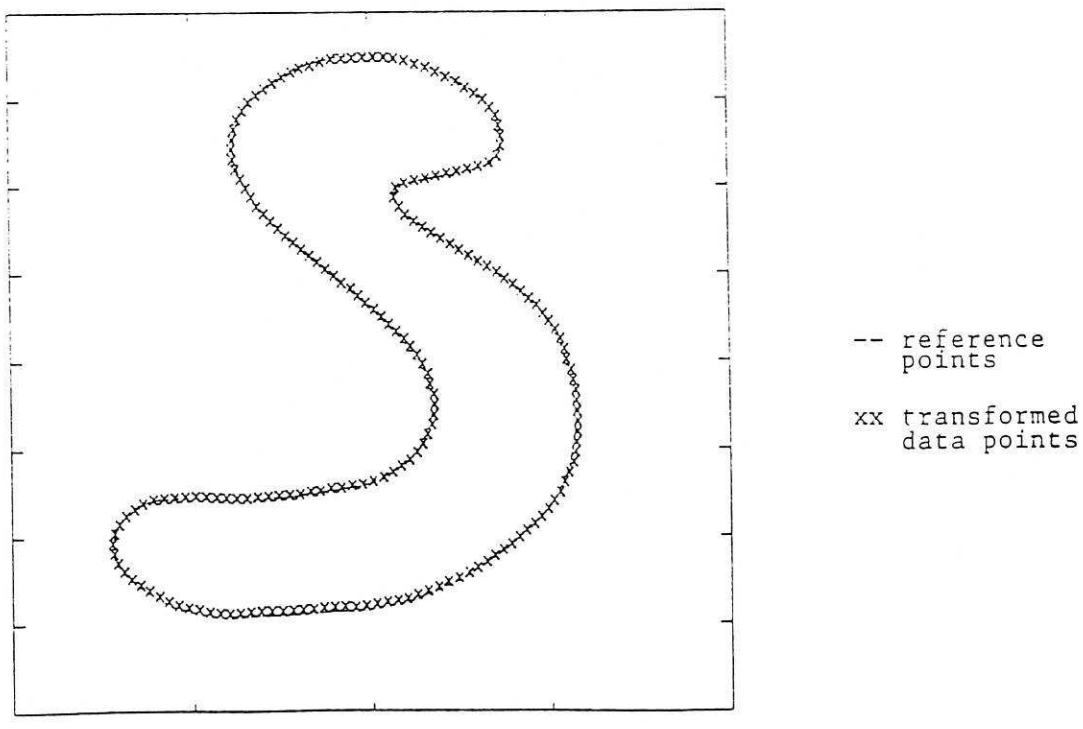

Figure 6. Transformed boundary data points superimposed on the reference data points

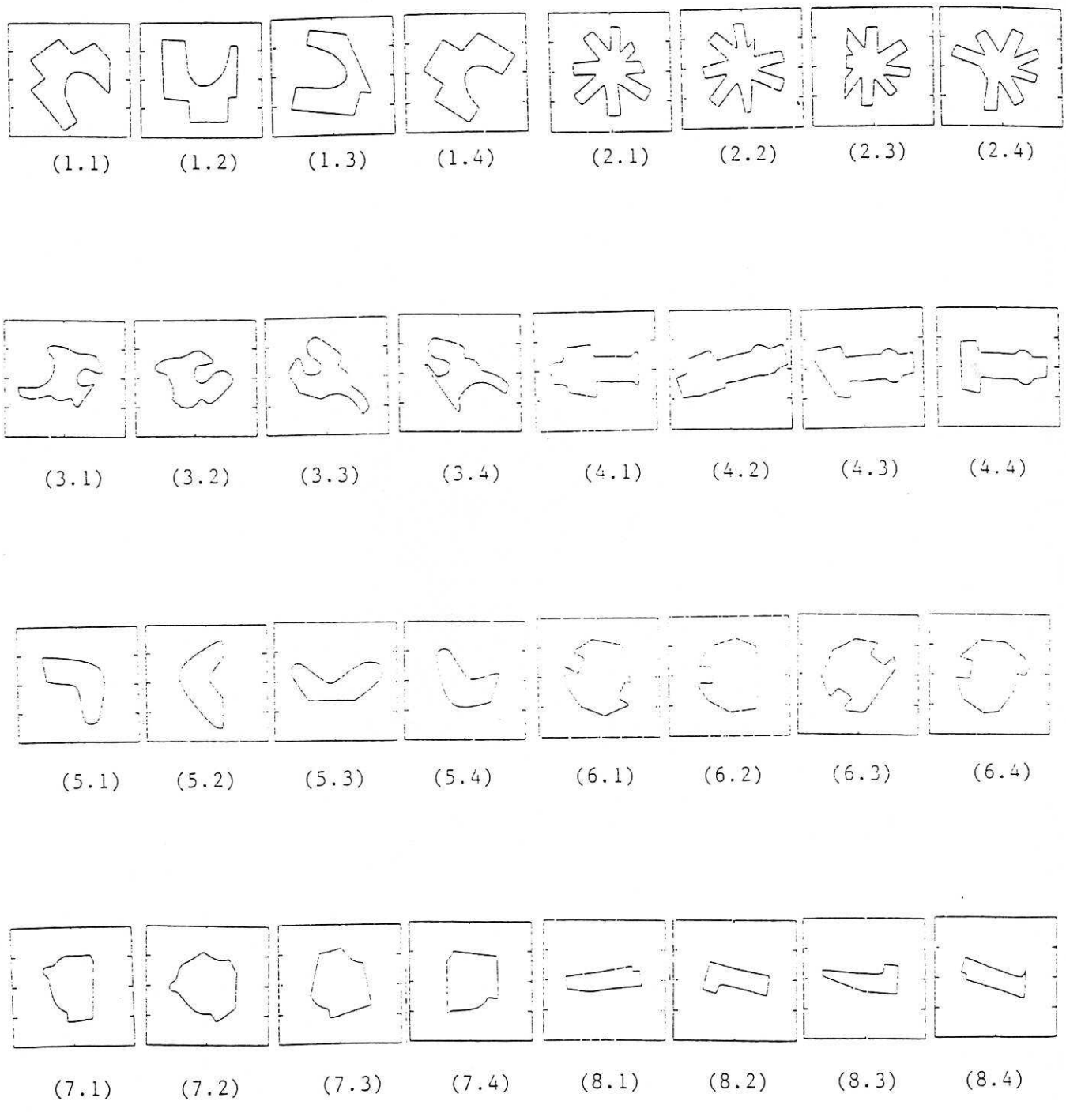

Figure 7. Shape set D